

Effect of Infill Masonry Walls on the Seismic Response of Reinforced Concrete Buildings Subjected to the 2003 Bam Earthquake Strong Motion : A Case Study of Bam Telephone Center

Hossein Mostafaei* and Toshimi Kabeyasawa

Earthquake Research Institute, The University of Tokyo

Abstract

The Bam telephone center building, with a nonsymmetrical reinforced concrete moment-resisting frame structure, is located about 1.5 km northeast of the 2003 Bam earthquake strong motion station. Based on post-earthquake damage assessment results, almost no residual deformations or cracks were observed in the structural elements of the building. However, assuming the designed base shear coefficient of the structure, nonlinear responses were expected due to the earthquake. Hence, to obtain an analytical answer for the almost linear performance of the building, 3-dimensional nonlinear time history analyses were carried out for north-south and east-west recorded strong motions. The response simulations were performed for different categories of bare frame and infilled frame. An approach was developed to model masonry infill walls with or without openings. The results of the analyses were compared to damage and residual cracks observed on the masonry infill walls. Reasonable correlations were obtained between analytical and observed results. It may be concluded that the presence of masonry infill walls is the main reason for the nearly linear responses of the Bam telephone center building during the earthquake.

Key words : Bam earthquake reinforced concrete building, nonlinear analysis, time-history analysis, and masonry infill wall

1. Introduction

The Bam telephone center building is a newly constructed 3-story nonsymmetrical reinforced concrete building located on Zeid square, N29.10° and E 58.37°, about 1.5 km North-East of the Bam strong motion station, which is operated by Building and Housing Research Center (BHRC). The peripheral and some of the internal frames of the building are infilled with masonry solid brick walls. Figs. 1 and 2 show overall building façade views and damage to infill masonry walls and façade walls. The photos were taken 1 month after the earthquake. Infill masonry walls were observed to have some diagonal and horizontal residual cracks. On the first floor, infill walls suffered higher levels of damage and cracks than the masonry walls on the basement and

second floors. This might be due to fewer walls on the first floor than on the other 2 floors. The façade masonry out-of-frame-walls were damaged due to relatively large drifts caused by the earthquake. Alternatively, almost no damage or residual cracking was observed on the structural elements, which might imply that the structure had almost linear performance during the earthquake. Based on the minimum base shear coefficient required by the Iranian seismic design code for such a building, as described later, this building may not perform linearly when subjected to the recorded strong motion. Therefore, a more detailed survey was carried out to evaluate the performance of the building during the earthquake. To find an analytical answer for such performance, 3D nonlinear time-history analyses are

* e-mail : Mhossein@eri.u-tokyo.ac.jp (1-1 Yayoi 1 chome, Bunkyo-ku, Tokyo, 113-0032 Japan) Kojiok@hiroshima-u.ac.jp

carried out by applying the Opensees program, Mazzoni S. *et al.* (2004). An approach was developed to obtain analytical models for the masonry infill walls with or without openings. Architectural and structural plans and details of the building were provided by the central communication office of Kerman province in Kerman city. The locations of the building and strong motion station in Bam city are shown in Fig. 3.

2. Object of the analysis

Structural engineers, during the design process of a building, typically, ignore the effects of infill masonry walls in the structural analysis. The only contributions of masonry infill walls are their masses as non-structural elements. Consequently, analyses of the structures are based on the bare frames. In the last 4 decades, the effects of infill walls in frame structures have been extensively studied. Experimental and analytical study results show that infill walls have a significant effect on both the stiffness and the strength of structures (Moghaddam and Dowling, 1987). Studies have also been done to obtain analytical models that consider the effects of infill walls in the analysis, by Madan *et al.* (1997). Therefore, in the present study, it is estimated that the infill masonry walls might have major effects on the building performance, leading the structure to perform almost linearly. Hence, attempts were made to employ a realistic approach to modeling the infill masonry walls in the analysis of the Bam telephone center structure. The building was modeled for 3 different categories. First, in the category of BF, Bare Frame, the 3D bare frame of the building without stiffness and strength contributions of the infill walls are considered. However, infill wall masses on each floor are added to the mass of the corresponding floor. Second, in the category of FIM, Frame and Infill Masonry, the 3D structure is modeled considering the effects of strength and stiffness of infill masonry panels, as well as their masses. Finally, in the category of FIL, Frame and Infill Light panel, the 3D bare frame is considered with a light partitioning system instead of infill masonry walls. The last category was selected to compare the roles of infill masonry walls and those of low-strength light panels in terms of structural performance. Structural designers principally complain about employing heavy

masonry walls as partitions in a building due to their large unit masses. Under the third category, an attempt is made to estimate structural responses if the heavy infill masonry walls are substituted with light partitioning materials. This might enhance structural performance and safety because the total mass of the structure is reduced. However, the strength of the new materials is sufficiently low to be neglected, and the reduced strength and stiffness of the infill masonry walls from the structure may lead the building to perform with a lower capacity than when partitioned with masonry walls.

3. Designed base shear coefficient of the building

The designed base shear coefficient is estimated to compare the expected response, derived from a single degree freedom response spectrum.

The minimum base shear force, based on the Iranian seismic code BHRC (1999-b), can be obtained as follows :

$$V = CW \quad (1)$$

where ; V : Shear force, W : Total Weight of Building + 20% live load (for this type of building) and C : seismic coefficient as $C = ABI/R$
A ; Design base acceleration (ratio of seismic acceleration to gravity acceleration g) = 0.3 for the zone in which the building is located. I ; Building important factor I = 1.2 because this building is for a communication facility. R ; Building behavior factor (ordinary moment resisting concrete frame) R = 5, B ; Building response factor obtained from a design response spectrum. It can be determined from the following equation ;

$$B = 2.5 (T_0/T)^{2/3} \leq 2.5$$

where, T_0 : A value selected by soil type, assuming soil type II ; $T_0 = 0.5$, T : Building fundamental period ; $T = 0.07H^{3/4}$ so $T = 0.51$, hence ; $B = 2.5$, Therefore, the seismic coefficient is obtained :

$$C = 0.3 \times 2.5 \times 1.2 / 5 = 0.18$$

To compare this value to the expected response of the structure due to the earthquake, the natural period of the building was obtained using the Opensees program, (Mazzoni S., *et al.*, 2004), and performing an eigen-value analysis. As a result, the fundamental periods were obtained as $T = 0.4$ and 0.7 for

Effect of Infill Masonry Walls on the Seismic Response of Reinforced Concrete Buildings Subjected to the 2003 Bam Earthquake Strong Motion : A Case Study of Bam Telephone Center



Fig. 1. Bam telephone center RC building after Dec. 2003 Earthquake, South and East sides.



Fig. 2. Bam telephone center RC building after Dec. 2003 Earthquake, North side.

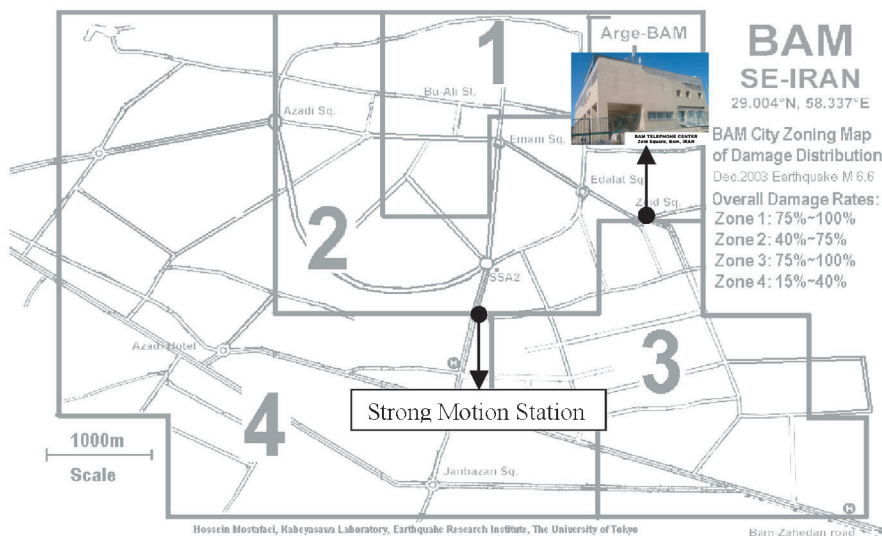


Fig. 3. Location of the Bam telephone center and the strong motion station on the Bam zoning map of building damage distribution.

the infilled frame structure, considering the effects of infill masonry walls, and for the bare frame structure, respectively. A SDOF response spectrum analysis was carried out for the recorded strong motion data. Maximum response accelerations for the 2 fundamental periods were obtained as 0.85 g for $T=0.4$ and 0.9 g for $T=0.7$. Comparing the maximum acceleration response coefficients (maximum acceleration responses/g) 0.85 and 0.9 with the seismic coefficient factor of $C=0.18$, it may be concluded that the structure must have a response to large nonlinear deformations due to the earthquake. However, based on post-earthquake observations, no significant residual cracks were observed on the structural elements, except the masonry walls, which implies nearly linear structural responses by the building. Soil structure interaction, site effect, uncertainty of strong motion, effects of infill masonry walls, and higher material strengths might be reasons for the unexpected response. Considering the dimensions of the building as a low-rise structure, the effects of the soil structure interaction may be neglected for this structure. Because the distance between the strong motion station and the building site is about 1500 m, and

both of them are located in the same damage level zone (Fig. 3), the same scale of strong motion as that recorded may be assumed for the site of the building. Consequently, the only effects that could cause remarkable changes in the response for the building are the effects of infill masonry walls and intrinsic material strengths and stiffness that might be higher than nominal ones.

4. Structural configurations and plans of the building

A reinforced concrete frame with moment-resisting connections is assumed for the structural system of the Bam telephone center. The building has 1 basement and 2 upper stories. Basement, ground floor, and top story plans of the building are illustrated in Fig. 4-a to Fig. 4-c. The figures show the positions of the infill masonry walls with their names labeled, as well as reinforced concrete columns and beams. In addition, the columns cross-section dimensions on each horizontal axis are indicated beside the left end of the axis. The only exception is axis C, where the column at the intersection of 1 and C axes has a cross-section dimension of 50×50 ,

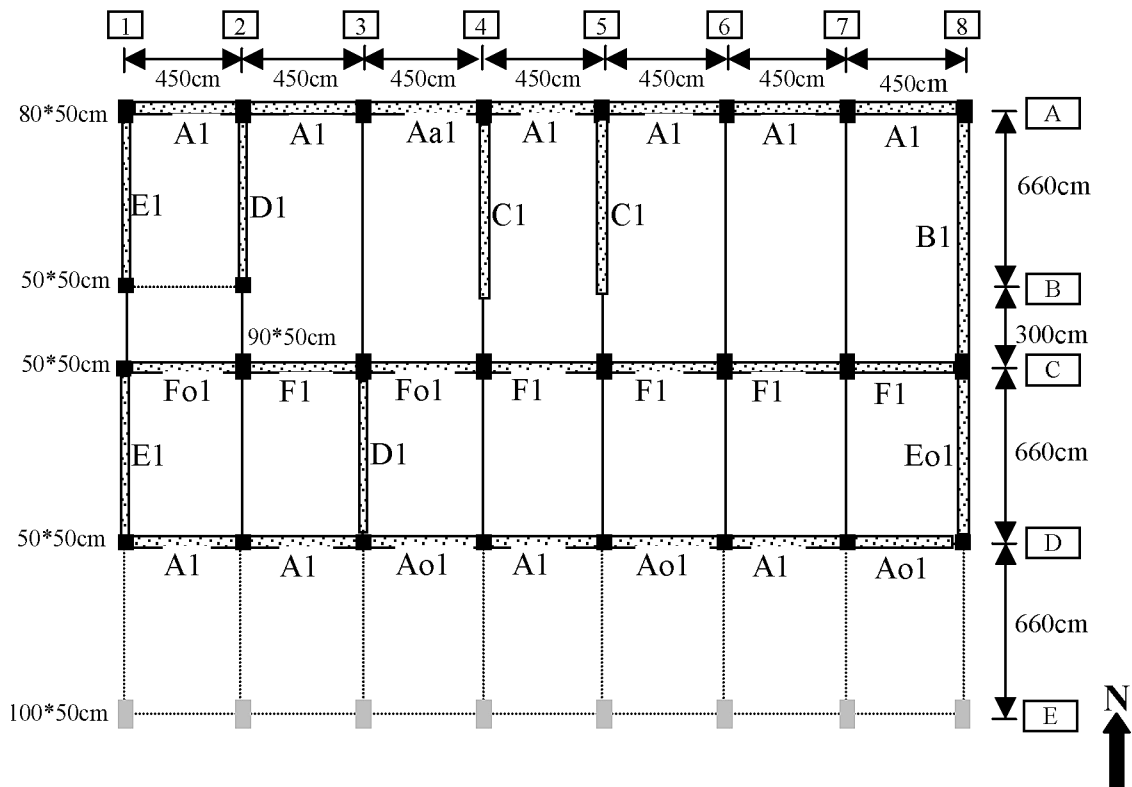


Fig. 4-a. Plan of Basement, Columns and Infill Walls.

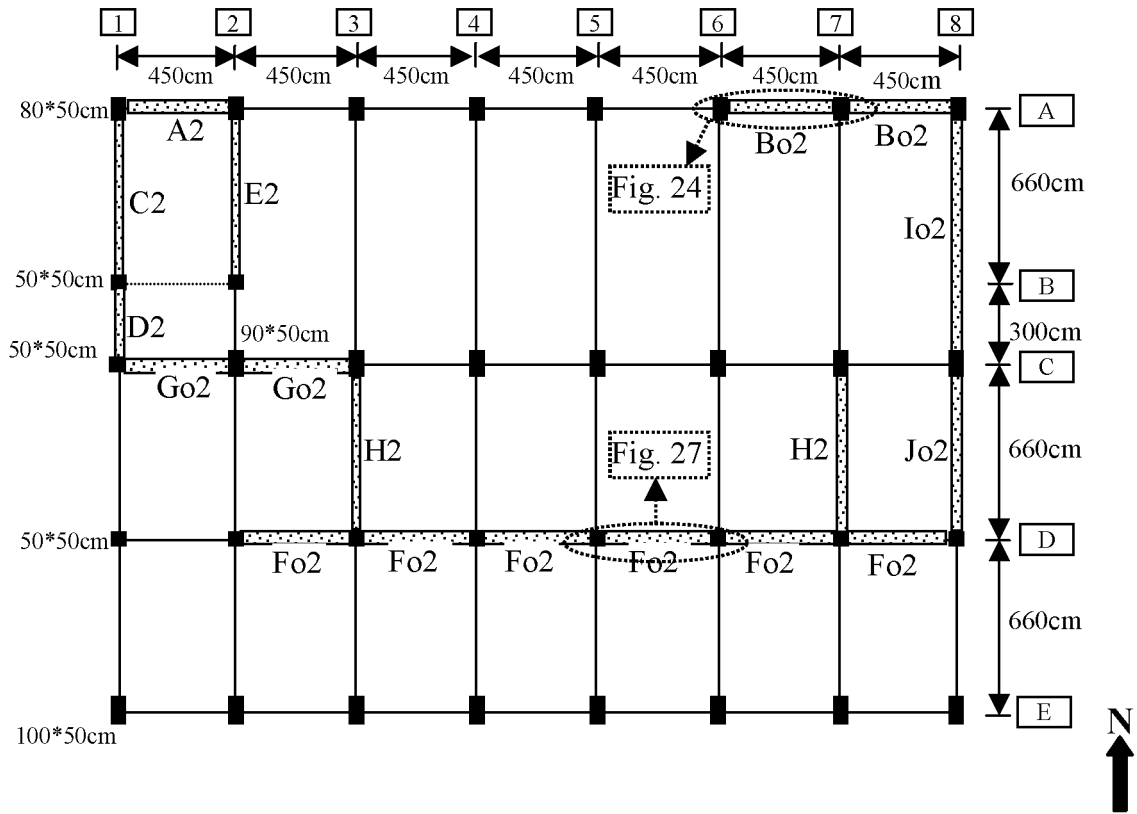


Fig. 4-b. Plan of Ground Floor, Columns, and Infill Walls.

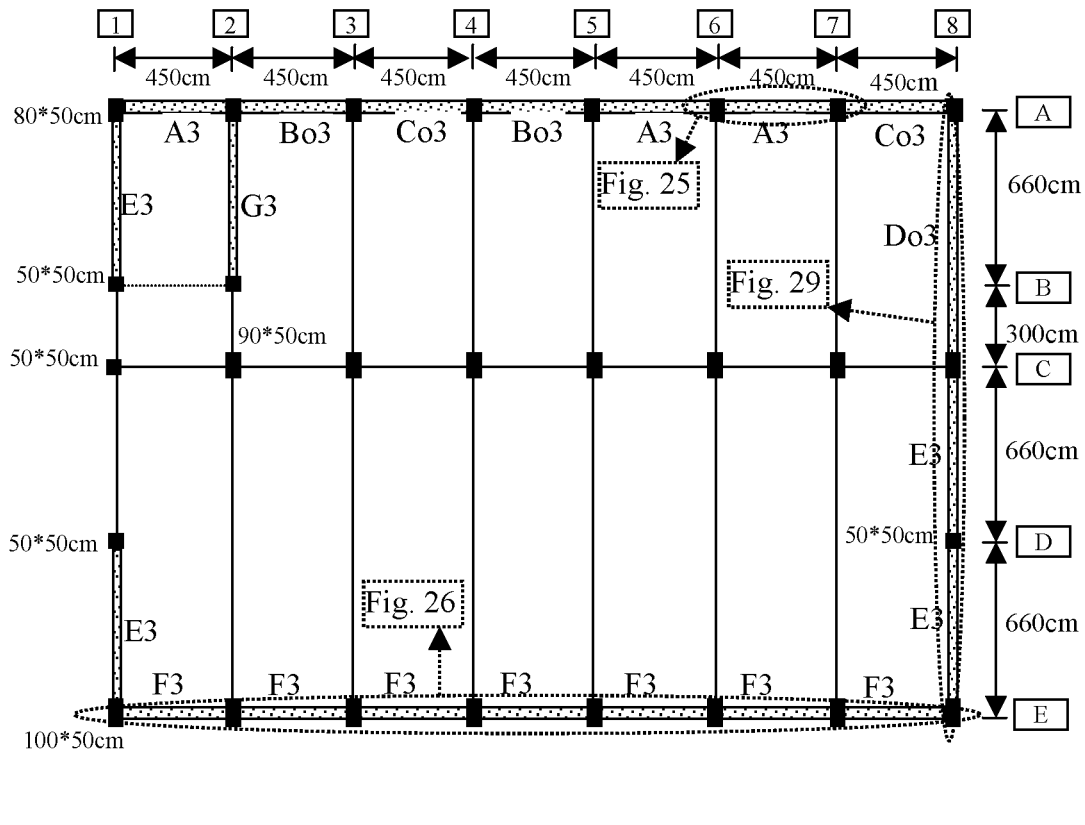


Fig. 4-c. Plan of Top Story, Columns, and Infill Walls.

however, the remaining columns on axis C have 90×50 cross-section dimensions.

Beam and column configurations on each frame are shown in Fig. 5, for frames in the north-south direction, and Fig. 6, for frames in east-west direction. For simplicity, mid-story tie-beams of the stairs are approximated by equivalent beams along the floors levels. Out of frames partition walls are not considered in the structural plans. However, they contribute to the total mass of the corresponding floors. Axis B has only 2 columns, assuming no beam, as shown in the plans.

5. Building weight computation

The weight of each floor was calculated from the summation of structural and non-structural elements weights. The weights of the infill walls were computed for each floor separately, and are added to the total weight. This was done to evaluate the effects of infill walls on structural behavior when different partitioning panels are applied instead of masonry walls, such as sandwich panels or other light materi-

als. For this purpose the light partitioning wall was assumed to have a unit weight of 65 kgf/m^2 (Unit weight of a solid brick masonry wall with a thickness of 22 cm is about 400 kg/m^2). The strengths of the new partitions are not applied in the analysis and only their masses contribute. Unit weights of different materials are based on the Iranian Design Load Code, BHRC (1999-a).

The unit weight for the reinforced concrete elements was considered to be equal to 2500 kg/m^3 . The weight of each story was determined by considering 50% of the weights of the columns at the story plus 50% of the weights of the columns at the lower story plus the weights of the slab and the beams, as well as the stairs weights. The weight computations for buildings with masonry infill walls and with the light partitioning walls are summarized in Tables 1 and 2, respectively.

6. Columns and beams details and materials

The cross-section dimensions of columns, as well as their reinforcements, are presented in Table 3.

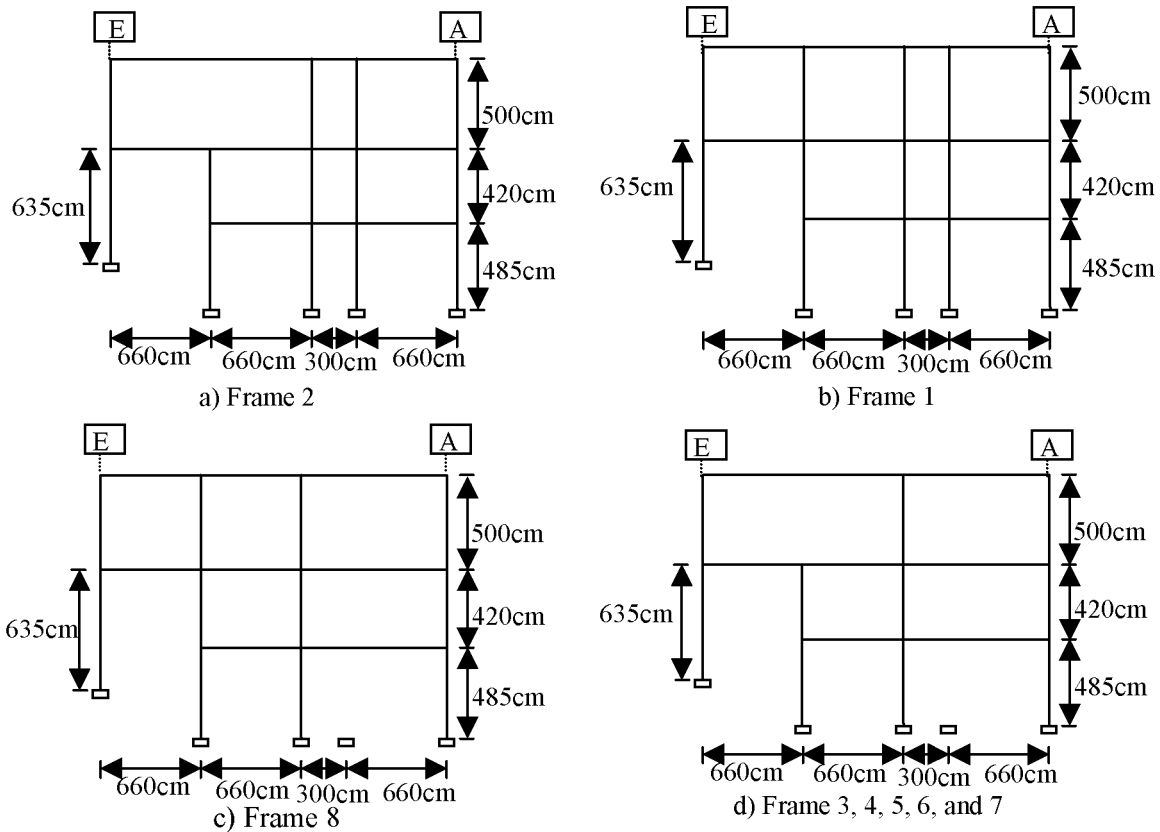


Fig. 5. North-South direction frames of the building.

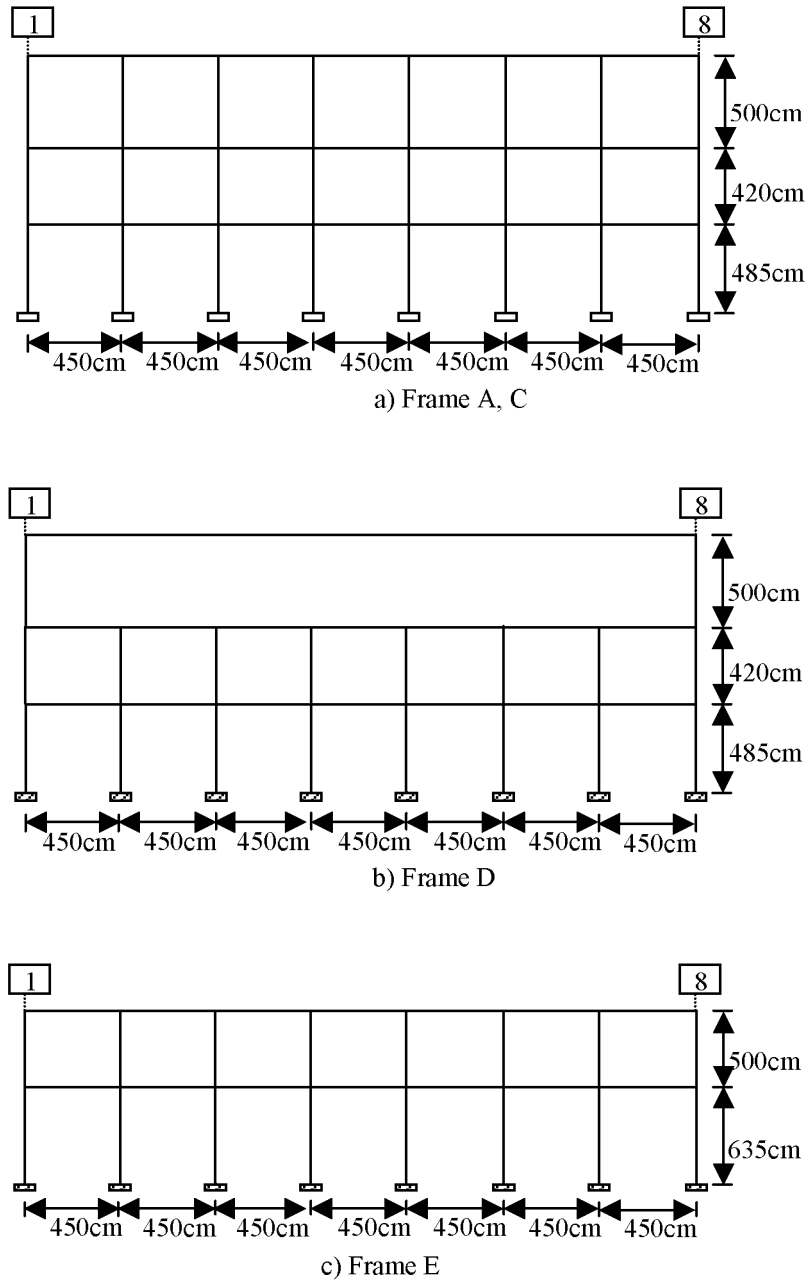


Fig. 6. East-West direction frames of the building.

Table 1. Summaries of weight computations for the building with masonry infill walls.

Story No.	Ground Floor	Middle Floor	Roof
Structure Weights kgf	443964	620265	635055
Flooring, Façade, and Partition walls Weights kgf	100677	100534	76535
Masonry infill walls Weights kgf	95804	249262	0
Assumed weights for instruments and furniture in the building	25000	30000	10000
Total Weights kgf	665445	1000061	721590

Stirrups for all of the columns are arranged at the 2 ends, each at a length of 1.5 m, as $3\phi 10@10$ and at the central part, the remaining length, as $3\phi 10@25$. In this study, for simplicity, the beams are presumed to have linear responses. Nonlinear deformations are considered to occur at the columns. This assumption can be verified after the analysis by comparing the responses to those of the linear state. For the case of a bare frame, BF, and a frame with a light partitioning material, FIL, large deformations are expected. This assumption is conservative because the observed performance of the building after the earthquake does not imply a considerable nonlinear defor-

mation of the structural elements. Therefore, reinforcements of the beams are not presented here. The flange widths, B_f , of the presumed T-shape beams sections are estimated from the AIJ recommendation (1994). Cross-section dimensions of beams are listed in Table 4. At roof level, parapet walls are erected on axes A, E, 1, and 8 along the top edge of the corresponding beams. The second moment inertias of the parapets are also added to the corresponding beams' moment inertias. The width and the height of the parapet are 150 mm and 1000 mm, respectively. The compression strength of concrete for the structural components is assumed to be 26 MPa, as the design

Table 2. Summaries of weight computations for the building with the assumed light partitioning walls.

Story No.	Ground Floor	Middle Floor	Roof
Structure Weights kgf	443964	620265	635055
Flooring, Façade, and Partition walls Weights kgf	100677	100534	76535
Light partition walls Weights kgf	14375	25022	0
Assumed weights for instruments and furniture in the building	25000	30000	10000
Total Weights kgf	584016	775821	721590

Note: Based on an interview with the building personnel, at the time of earthquake, the building was almost empty and no one worked there. Therefore, the corresponding portion of the live load can be neglected for the evaluation state.

Table 3. Dimensions and reinforcements of the columns.

No.	Locations: Axis Intersection	W×H mm (cross-section dimensions)	Longitudinal Bars, n+m Φ d		
			1 st	2 nd	3 rd
C1	C-2 to C-7	500×900	10+6 Φ 26	8+6 Φ 24	8+6 Φ 24
C2	A-2 to A-7	500×800	8+6 Φ 26	8+6 Φ 24	8+6 Φ 24
C3	E-1 to E-8	500×1000	N/A	10+6 Φ 28	10+6 Φ 26
C4	D-2 to D-7	500×500	8+4 Φ 22	8+4 Φ 22	N/A
C5	A-1 and A-8	500×800	10+4 Φ 26	8+4 Φ 22	8+4 Φ 22
C6	B-1&B-2&C-1	500×500	8+4 Φ 26	8+4 Φ 26	8+4 Φ 26
C7	D-1 and D-8	500×500	8+4 Φ 22	8+4 Φ 22	8+4 Φ 20
C8	C-8	500×900	8+6 Φ 24	8+6 Φ 24	8+6 Φ 26

1st= Basement, 2nd =Ground Floor, and 3rd =Top Story, W: Width (in east-west direction), H= Height (in north-south direction), n, and m, number of bars on the two W sides and number of bars on the two H sides, as shown in the following cross-section. d: diameter of the bars (mm), N/A= not applicable

Stirrups arrangements in the columns:
 $2\phi 10@10$ for the two ends and $2\phi 10@25$ for the center part
 $1\phi 10@10$ for the two ends and $1\phi 10@25$ for the center part

nominal value, derived from the structural map. Confinement effect was employed for the compression strength of the concrete cores of columns, and calculated to be equal to 33 MPa based on the method proposed by Mander *et al.* (1988). The yielding stress of the steel bars is derived, from the structural map, as $f_y = 3000 \text{ kg/cm}^2$.

7. Masonry infill walls

Infill walls in the Bam telephone center building can be generally categorized into 3 types : masonry infill walls with solid bricks, as shown in Fig. 7, hollow block walls, as shown in Fig. 8, and multipart masonry-concrete infill walls. The hollow block walls contribute just to the total mass of the building and their strengths and stiffness are neglected, because most of them were out of frames. The last type is a form of peripheral wall in the basement of the building, in which a 330 cm height-reinforced concrete wall (thickness of 25 cm) was erected at each bay, as shown in the footnote to Table 5. The upper parts of the bays, above the reinforced concrete walls, are filled with masonry walls. Table 5 details

all of the infill panels contributing to structural performance. Masonry walls Aa1 and Eo1 have full openings on the upper part.

The compression strength of the masonry prism, f'_p , is determined from an equation recommended by Paulay and Priestly (1992) as :

$$f'_p = \frac{f'_{cb}(f'_{tb} + \alpha f'_j)}{U_u(F'_{tb} + \alpha f'_{cb})}, \text{ where } \alpha = \frac{j}{4.1h_b}, \text{ and } U_u = 1.5 \quad (2)$$

where, f'_{tb} = tension strength of the brick, f'_{cb} = compression strength of the brick, f'_j = mortar compression strength, h_b = the height of the masonry unit (in this study height of a solid brick) $h_b = 60 \text{ mm}$, j = the mortar joint thickness = 15 mm, and U_u is the stress non-uniformity coefficient equal to 1.5.

Solid hand-made clay bricks are used for the infill walls of the building. Based on a post-earthquake investigation of quality control for bricks in the Bam area, implemented by Building and Housing Research Center of Iran, an average of $f'_{cb} = 75 \text{ kg/cm}^2$ may be assumed for the compression strength of the bricks in the selected building. Based on struc-

Table 4. Beam reinforcements and cross-section dimensions.

Beams Axis	Intersectional Axes	Story	Width (mm)	Height (mm)	Effective Width Bf (mm)	Slab Depth (mm)	Parapet Walls (mm)
A, E	All beams	1 st , 2 nd	500	500	950	160	N/A
A, E	All beams	3 rd	500	500	950	160	150×1000
C, D	All beams	1 st , 2 nd , 3 rd	500	500	1400	160	N/A
1	A to B and C to E	1 st , 2 nd	500	800	1160	160	N/A
1	B to C	1 st , 2 nd	500	800	800	160	N/A
1	A to B and C to E	3 rd	500	1000	1160	160	150×1000
1	B to C	3 rd	500	1000	800	160	150×1000
2	A to B and C to E	1 st , 2 nd	500	800	1820	160	N/A
2	B to C	1 st , 2 nd	500	800	1100	160	N/A
2	A to B	3 rd	500	1000	1820	160	N/A
2	B to C	3 rd	500	1000	1100	160	N/A
2	C to E	3 rd	500	1000	2880	160	N/A
3 to 7	A to C	1 st , 2 nd	500	800	2460	160	N/A
3 to 7	C to E	1 st , 2 nd	500	800	1820	160	N/A
3 to 7	A to C	3 rd	500	1000	2460	160	N/A
3 to 7	C to E	3 rd	500	1000	2880	160	N/A
8	A to C	1 st , 2 nd	500	800	1480	160	N/A
8	C to E	1 st , 2 nd	500	800	1160	160	N/A
8	A to C	3 rd	500	1000	1480	160	150×1000
8	C to E	3 rd	500	1000	1160	160	150×1000

1st = Roof of the basement, 2nd = Roof of the ground floor, and 3rd = Roof of the top story.

tural detail maps, the cement-sand ratio of the mortar is 1 : 5. The corresponding compression strength of the mortar is considered to be 50 kg/cm², which is derived from experimental results on the same cement-sand ratio, carried out by Moghaddam (2004).

The tension strength of the solid bricks may be determined as, (T. Paulay, M.J.N. Priestly, 1992) :

$$f'_{tb} = 0.1f'_{cb}, \text{ therefore, } f'_{tb} = 7.5 \text{ kg/cm}^2$$

Hence, compression strength of a masonry prism is obtained as :

$$f'_b = \frac{75(7.5 + \alpha 50)}{1.5(7.5 + \alpha 75)}, \text{ where } \alpha = 0.061 \Rightarrow f'_b = 44 \text{ kg/cm}^2$$

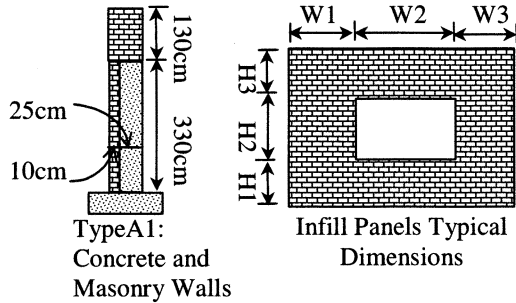
8. Shear strength of infill walls

There are several potential failure modes for infill masonry walls, Paulay, and Priestley (1992), in-

Table 5. Infill walls Dimensions.

No	W1 cm	W2 cm	W3 cm	H1 cm	H2 cm	H3 cm	t _m cm	t _c
A1	400	0	0	330	0	130	35	25 cm
Aa1	400	0	0	330	0	0	35	25 cm
Ao1	85	230	85	330	130	0	35	25 cm
B1	875	0	0	330	0	100	35	25 cm
C1	660	0	0	430	0	0	22	0
D1	595	0	0	430	0	0	22	0
E1	595	0	0	330	0	100	35	25 cm
Eo1	595	0	0	330	0	0	35	25 cm
F1	400	0	0	460	0	0	22	0
Fo1	185	180	35	0	220	240	22	0
A2	400	0	0	370	0	0	35	0
Bo2	70	260	70	90	140	140	35	0
C2	595	0	0	340	0	0	35	0
D2	250	0	0	340	0	0	35	0
E2	595	0	0	340	0	0	22	0
Fo2	85	230	85	90	140	140	35	0
Go2	265	100	35	0	220	150	22	0
H2	590	0	0	340	0	0	22	0
Io2	120	635	120	90	140	110	35	0
Jo2	590	0	0	90	140	110	35	0
A3	400	0	0	450	0	0	35	0
Bo3	17	130	253	90	140	220	35	0
Co3	70	260	70	90	140	220	35	0
Do3	240	395	240	90	140	170	35	0
E3	595	0	0	400	0	0	35	0
F3	400	0	0	450	0	0	35	0
G3	595	0	0	400	0	0	22	0

No: Infill wall labels in the floor plans, t_m: thickness of the masonry walls t_c: thickness of the reinforced concrete infill wall (at the basement, periphery wall is multipart: RC & masonry walls)



Alternatives of infill-panel types and dimensions:

1. For infill panels without opening: W2=W3=H2=H3=0
2. For infill panels with door opening: H1=0
3. For infill panels with top: a masonry wall and bottom: a concrete wall (periphery basements walls): W2=W3=H2=0
4. For infill panels with two or three openings, average values are applied, since-

there are few cases: W2= summation of openings (windows) widths, W1= summation of walls widths from center to the left side of the panel, W3= summation of walls widths from center to right side of the panel, all openings are in the same levels



Fig. 7. Solid brick masonry walls in the Bam telephone center building.



Fig. 8. Hollow block walls in the Bam telephone center building.

cluding :

1. Sliding shear failure of masonry walls, horizontally
2. Compression failure of diagonal strut
3. Diagonal tensile cracking. This is not a general failure. Higher lateral forces can be supported by the above failure modes.
4. Tension failure mode (flexural), which is not usually a critical failure mode for infill walls

Shear strengths for the first and second critical types of failure mode are obtained for each infill panel, and the minimum value is considered to be the shear strength of the infill wall.

8.1 Sliding shear failure

The Mohr-Coulomb failure criteria can be applied to assess the maximum shear strength for this kind of failure mechanism :

$$\tau_f = \tau_o + \mu \sigma_N \quad (3)$$

where, τ_o = cohesive capacity of the mortar beds, μ = sliding friction coefficient along the bed joint, and σ_N is vertical compression stress in the infill walls.

Applying the panel dimension, maximum horizontal shear force V_f is assessed as follows :

$$V_f = \tau_o t l_m + \mu N \quad (4)$$

where, t = infill wall thickness, l_m = length of infill panel, and N vertical load in infill walls. In FEMA 306 (1998), N is determined to be the vertical load applied by vertical shortening strain in the panel due to lateral drifts.

$$N = l_m t E_m r^2 \quad (5)$$

where, E_m = Young's modulus of the masonry, and r is the interstory drift angle.

In this study, N is estimated directly as a summation of applied external vertical load on the panel and the vertical component of the diagonal compression.

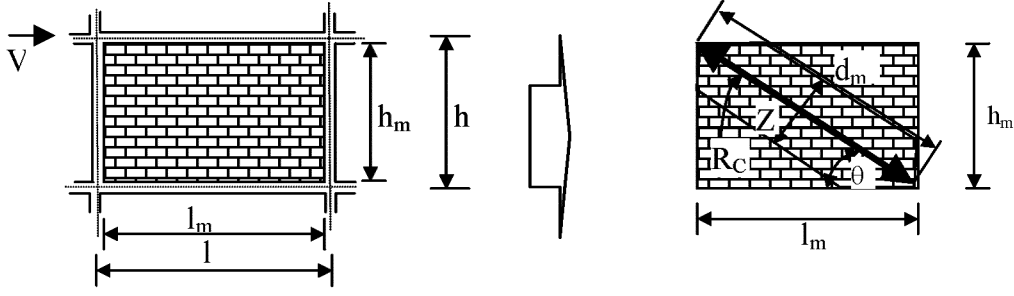


Fig. 9. Infill masonry walls and the equivalent diagonal compression action parameters.

sion force R_c , as shown in Fig. 9. The external vertical load is zero for the infill walls of the building, and only the vertical component of the strut compression force is considered.

Therefore, maximum shear force can be calculated as : Substituting $V_f = R_c \cos\theta$, the horizontal component of shear force R_c in Fig. 9, into the above equation produces :

$$R_c \cos\theta = \tau_o t l_m + \mu R_c \sin\theta$$

$$\text{Or, } V_f = \frac{\tau_o t l_m}{(1 - \mu \tan\theta)} \quad (6)$$

Typical ranges of τ_o are $1 \leq \tau_o \leq 15 \text{ kg/cm}^2$. For evaluation analysis purposes, it may be assumed typically as $\tau_o = 0.04 f'_m = 0.04 * 44 = 1.76 \text{ kg/cm}^2$ (Paulay and Priestley, 1992). As for μ , it is determined from the experimental results of Chen (2003) in the following equations :

$$\mu = 0.654 + 0.000515 f'_j \quad (7)$$

where, f'_j is the mortar block compression strength (kg/cm^2), which is 50 kg/cm^2 as mentioned before. Based on the above equation and $f'_j = 50 \text{ kg/cm}^2$, mortar compression strength, the friction coefficient is calculated as $\mu = 0.68$. Therefore, the maximum shear strength for each panel of the selected building, based on the sliding shear failure mechanism, can be obtained as :

$$V_f = \frac{1.76 t l_m}{(1 - 0.68 \tan\theta)} \quad (8)$$

8. 2 Compression failure

Compression failure of infill walls occurred due to the compression failure of the equivalent diagonal strut. The shear force (horizontal component of the diagonal strut capacity) can be calculated from an equation suggested by Stafford-Smith and Carter

(1969), however, the equivalent strut width Z , in Fig. 9, is computed using a modification recommended by FEMA 306 (1998).

$$V_c = z t f'_m \cos\theta \quad (9)$$

where,

f'_m = Masonry compression strength, which for ungrouted clay brick masonry, (Paulay and Priestley, 1992) :

$$f'_m = f'_b = 44 \text{ kg/cm}^2 = 4.4 \text{ MPa}$$

and z = equivalent strut width obtained by the following equation FEMA 306 (1998) :

$$Z = 0.175 (\lambda h)^{-0.4} d_m \quad (10)$$

where

$$\lambda = \left[\frac{E_m t \sin 2\theta}{4 E_c I_g h_m} \right]^{\frac{1}{4}}$$

and h = column height between centerlines of beams, cm, h_m = height of infill panel, cm, E_c = expected modulus of elasticity of frame material, = 240000 kg/cm^2 , E_m = expected modulus of elasticity of infill material, = $750 f'_m = 33000 \text{ kg/cm}^2$, Paulay, and Priestley, (1992), I_g = moment of inertial of column, cm^4 , d_m = diagonal length of infill panel, cm, t = thickness of infill panel and equivalent strut, cm, θ = angle whose tangent is the infill height-to-length aspect ratio, as :

$$\theta = \tan^{-1} \left(\frac{h_m}{l_m} \right)$$

where, l_m = length of infill panel

8. 3 Diagonal tensile cracking

Diagonal tensile cracking is not a general failure. Higher lateral forces can be supported by the other failure modes, Saneinejad, and Hobbs, (1995). However, it is regarded as a serviceability limit state, and

is defined as :

$$H_i = 2\sqrt{2} t h_m f_t \cos\theta \sin\theta \quad (11)$$

where, f_t = cracking capacity of masonry, $f_t \approx 0.166 \sqrt{f'_p}$, where, f'_p is the compression strength of the masonry prism MPa :

8.4 Maximum shear strength of masonry infill walls

The shear strengths obtained from the above failure modes, sliding shear failure and diagonal compression failure, may not exceed 8.3 kg/cm^2 , as recommended by ACI 530-88. Therefore, the corresponding shear strengths cannot be beyond the following value.

$$V_{\max}/t l_m = 8.3 \text{ kg/cm}^2 \quad (12)$$

9. Modeling of masonry infill walls

A masonry infill panel can be modeled by replacing the panel with a system of 2 diagonal masonry compression struts, Madan (1997). By ignoring the tensile strength of the infill masonry, the combination of both compression components provides a lateral load-resisting mechanism for the opposite lateral directions of loading. Fig. 10 shows the analytical model and the strength envelope for masonry infill walls.

The main factors of the envelope model, in Fig. 10, are shear strengths at the assumed yielding point, V_y , at the maximum point V_m , and the post-peak residual shear strength, V_p , and their corresponding displacements, U_y , U_m , and U_p , respectively. In the figure, α is the ratio of stiffness after yielding to that of the initial stiffness. To obtain the main parameters of the envelope curve, maximum lateral strength, V_m , should be estimated considering the 2 critical failure modes, sliding shear and compression failures, as mentioned in section 8. The other factors can be approximated from the following equations. The maximum displacement at the maximum lateral force is estimated by equation (13), Mandan *et al.* (1997) :

$$U_m = \frac{\epsilon'_m d_m}{\cos\theta} \quad (13)$$

where, ϵ'_m is the masonry compression strain at the maximum compression stress ; here $\epsilon'_m = 0.0018$, and d_m is the diagonal strut length. The maximum drift

limitation of 0.8% is applied for the U_m/h_m ratio, which is implied from the experimental results, Mehrabi *et al.* (1996) and Chen, (2003). The initial stiffness K_0 can be estimated by the following equation, Mandan *et al.* (1997) :

$$K_0 = 2(V_m/U_m) \quad (14)$$

The lateral yielding force V_y , and displacement U_y may be calculated from the geometry in Fig. 10 :

$$V_y = \frac{V_m - \alpha K_0 U_m}{1 - \alpha} \quad (15)$$

$$U_y = \frac{V_y}{K_0} \quad (16)$$

Here, the value of α is assumed to be equal to 0.2.

U_p and V_p can be defined from the previews of experimental results. The average value of drift ratio at the 80% post-peak point, defined as a point on the envelope curve, in Fig. 39, with a shear level 80% of the maximum shear strength, is about 1.5% for concrete block infill walls, Mehrabi *et al.*, (1996). It is assumed as $(3/4) 1.5\% = 1\%$, for solid bricks walls. The V_p and U_p should be determined considering that the line connecting the peak of the envelope and the point (V_p, U_p) passes through the 80% post-peak point. Therefore :

$$\text{Assuming ; } V_p = 0.3 V_m \quad (17)$$

$$\text{It may lead to : } U_p = 3.5(0.01 h_m - U_m) \quad (18)$$

To show the applicability of the horizontal spring model instead of a diagonal spring model, an example of one-bay frame with an infill masonry wall is presented here. The infilled frame is analyzed with both horizontal and diagonal models. Pushover analyses were employed for the 2 infilled frame models in Fig. 11.

The infill wall has the same details as the infill wall A2 in Table 5. The lateral force capacity, for this wall in the compression failure mechanism, can be calculated from equation (9) as : $V_c = z t f'_m \cos\theta$

$$\text{where } \theta = \tan^{-1}\left(\frac{h_m}{l_m}\right) = \tan^{-1}\left(\frac{370}{400}\right) = 42.76^\circ$$

$$\lambda = \left[\frac{E_m t \sin 2\theta}{4 E_c I_g h_m} \right]^{1/4} = \left[\frac{33000 \times 35 \sin 2\theta}{4 \times 240000 \times 833333 \times 370} \right]^{1/4}$$

$$= 0.0079 \quad E_m = 750 f'_m$$

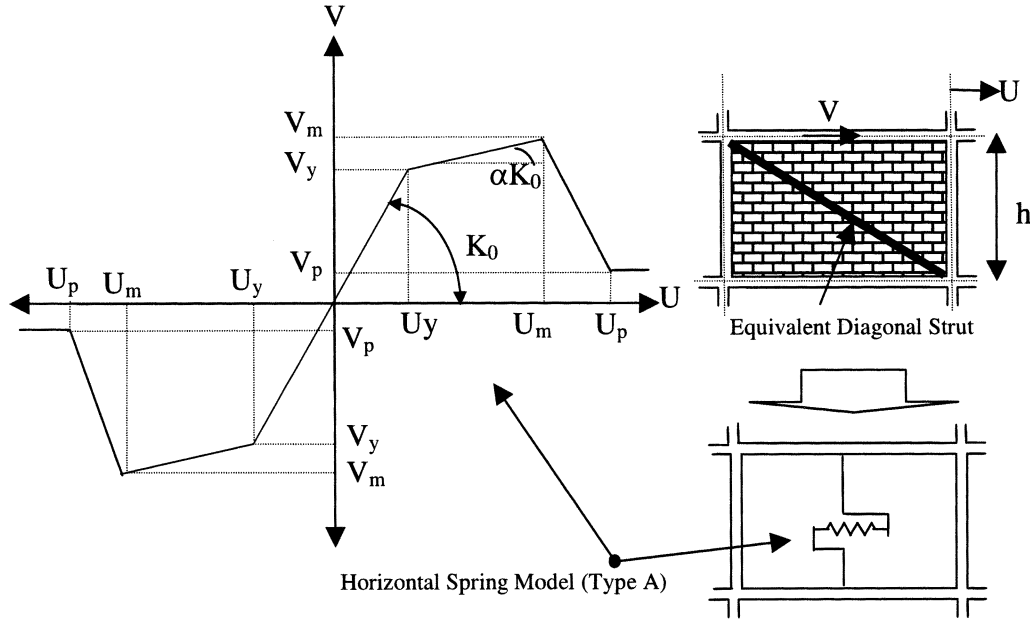


Fig. 10. Strength envelope for conventional masonry infill walls and the analytical model (Type A).

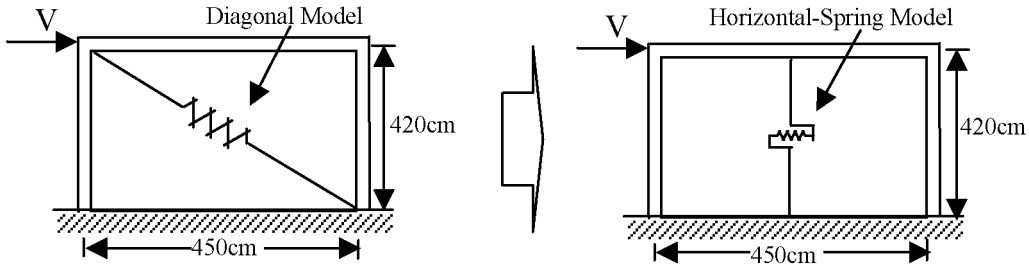


Fig. 11. Diagonal-spring and horizontal-spring as two masonry infill wall models.

$$z = 0.175(\lambda h)^{-0.4} d_m = 0.175 \times (0.0079 \times 420)^{-0.4} 545 = 59.03$$

$$V_c/tl_m = zt f'_m \cos\theta / tl_m = 59.03 \times 35 \times 44 \times 0.73 / 35 \times 400 = 4.77 \text{ kg/cm}^2$$

Lateral force assuming the sliding shear failure is determined by equation (8) :

$$V_f/tl_m = \frac{\tau_o}{(1 - \mu \tan\theta)} = \frac{1.76}{(1 - 0.68 \times 0.925)} = 4.74 \text{ kg/cm}^2$$

Selecting the minimum shear strength from the 2 mechanisms :

$$V_m = 4.74 \times 400 \times 35 = 66360 \text{ kgf.}$$

$$\text{From equation (13) : } U_m = \frac{\epsilon'_m d_m}{\cos\theta} = \frac{0.0018 \times 545}{0.73} = 1.344 \text{ cm}$$

The initial stiffness K_0 can be estimated as (equation 14) :

$$K_0 = 2(V_m/U_m) = 2(66360/1.344) = 98750 \text{ kg/cm}^2$$

The lateral yielding force V_y , and displacement U_y are (equations 15, 16) :

$$V_y = \frac{V_m - \alpha K_0 U_m}{1 - \alpha} = \frac{66360 - 0.2 \times 98750 \times 1.344}{1 - 0.2} = 49770 \text{ kgf}$$

$$U_y = \frac{V_y}{K_0} = \frac{49770}{98750} = 0.504 \text{ cm}$$

By applying equations 17 and 18 : $V_p = 0.3V_m = 19908$ kgf, $U_p = 3.5(0.01 h_m - U_m) = 8.25$ cm. As for the equivalent diagonal strut model, the area of the strut determined to be equal to $A_d = zt = 59.03 \times 35 = 2066.75 \text{ cm}^2$, and the envelope strain-stress curve are estimated as : $\sigma_y = V_y / (A_d \cos\alpha)$, $\sigma_m = V_m / (A_d \cos\alpha)$, $\sigma_p = V_p / (A_d \cos\alpha)$, where $\alpha = \tan^{-1}(420/450) = 43.03^\circ$, $\epsilon_y = U_y \cos\alpha / L_d$, $\epsilon_m = U_m \cos\alpha / L_d$, $\epsilon_p = U_p \cos\alpha / L_d$

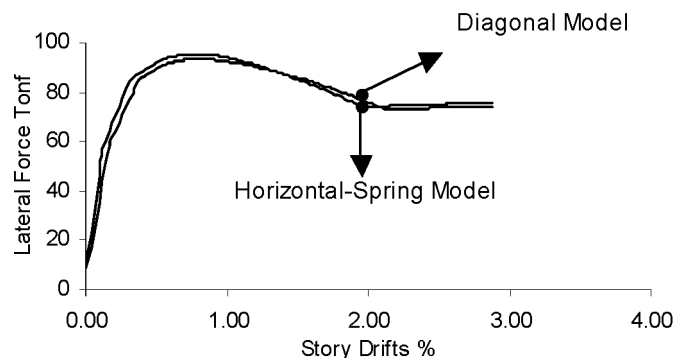


Fig. 12. Results of pushover analyses for the horizontal and diagonal infill wall models.

where

$$L_d = \sqrt{l^2 + h^2} L_d = \sqrt{450^2 + 420^2} = 616.5 \text{ cm}$$

Therefore : $\sigma_y = 32.9404 \text{ kg/cm}^2$, $\sigma_m = 43.9206 \text{ kg/cm}^2$, $\sigma_p = 13.12 \text{ kg/cm}^2$ and $\varepsilon_y = 0.0005986$, $\varepsilon_m = 0.001596$, and $\varepsilon_p = 0.00983$

For the analysis, the boundary columns and the 2 horizontal and diagonal infill wall models were configured with fiber models and zero lengths elements, respectively, in the Opensees program, and a nonlinear pushover analysis was used for each of the 2 models. A hysteretic model, which constructed a uniaxial bilinear hysteretic material object with pinching of force and deformation, damage due to ductility and energy, and degraded unloading stiffness based on ductility, was selected for the infill walls springs in this study. The envelope parameters of the hysteretic models are shown in Fig. 10.

The relationship between lateral drifts and lateral forces for the infilled frames are obtained, and the outcomes for both models are illustrated in Fig. 12. As the figure shows, the 2 models have almost the same responses. Therefore, it might be implied that each of the 2 models can be applied for evaluating the performance of infilled frames. In this study, all of the infill walls are modeled from the horizontal spring model. This model can be simply applied to infill walls with openings by means of multipart-infill or multi-spring models.

Different infill wall models are developed for different opening types. Figs. 13-a to 13-g illustrate the different spring models for infill walls with windows and doors openings, as well as infill complex RC-masonry walls. Springs for infill walls with different stiffnesses in the vertical direction, such as those

in Figs. 13-a to 13-f, are constrained to the corresponding nodes along the column lengths. This can be done by decomposing the column into 2 or 3 sub-elements, depending on the number of infill walls sub-elements in the vertical direction. For example, boundary columns of the infill walls in Fig. 13-a are divided into 3 column sub-elements by introducing 2 extra nodes along the columns. The horizontal springs are constrained to the corresponding nodes on the column sub-elements. The horizontal lines between the extra nodes illustrate the constraining paths without any other effect on the structural stiffness. The horizontal springs may be constrained to the corresponding nodes on the columns for compression only, in the case of assuming zero tensile strength at the interface nodes.

10. Equivalent Models for Multi-springs panels

For simplicity, an equivalent model can be applied in the analysis process instead of several spring models for an infill walls with openings or multipart infill walls, such as the models illustrated in Fig. 13-a to 13-g. In this study, different types of infilled frame of the building were assessed individually, considering the type of corresponding infill wall. The result obtained is assumed to be the equivalent single spring model of the infill wall. The equivalent model can be obtained by doing pushover analyses for the individual frames with and without an infill wall. Subsequently, the lateral force-displacement envelope curve response of the bare frame will be deducted from that of the corresponding multi-spring infilled frame. The force-displacement curve obtained is the equivalent envelope for the single spring model, which can be easily applied as type A

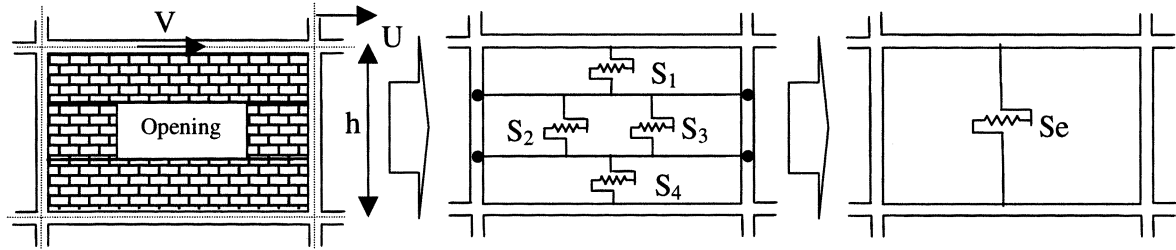


Fig. 13-a. Infill masonry walls with one window-opening Type B.

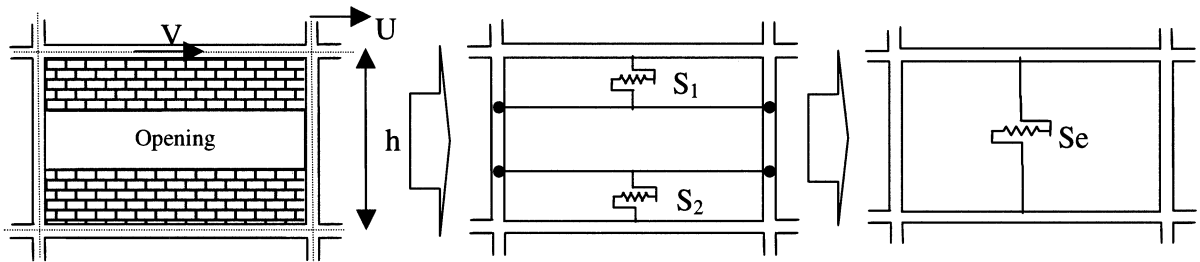


Fig. 13-b. Infill masonry walls with one mid-full-opening Type C.

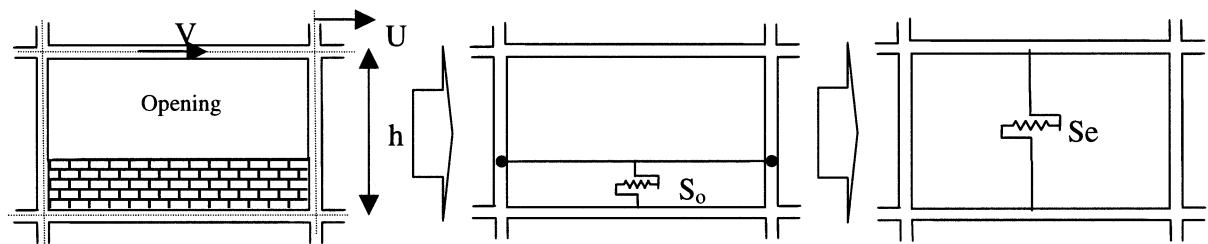


Fig. 13-c. Infill masonry walls with one up-full-opening Type D.

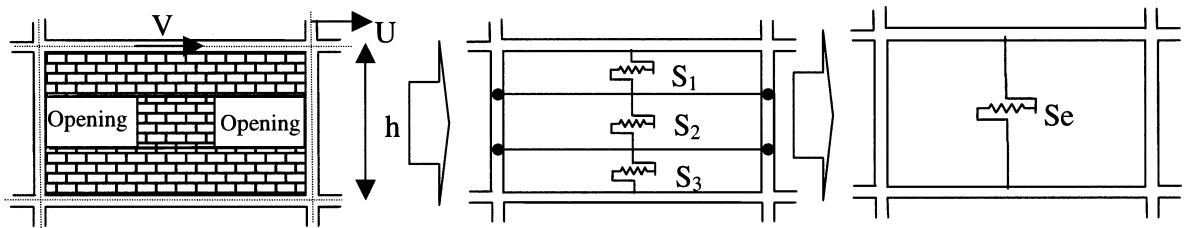


Fig. 13-d. Infill masonry walls with two mid windows opening Type E.

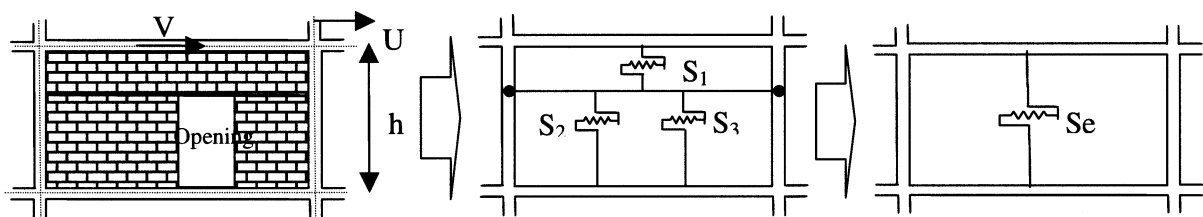


Fig. 13-e. Infill masonry walls with one-door-opening Type F.

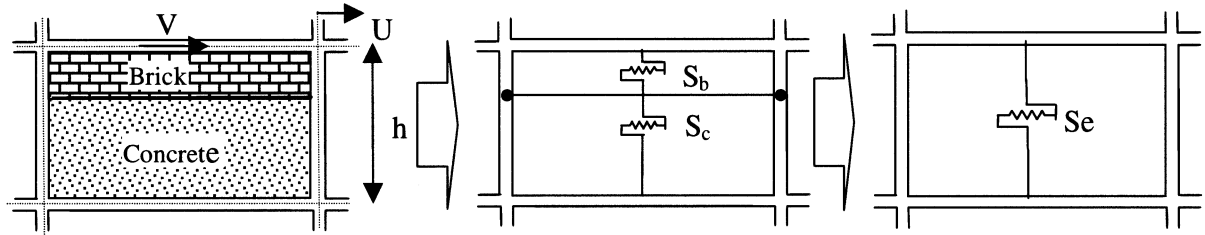


Fig. 13-f. Infill horizontally multipart masonry walls Type G.

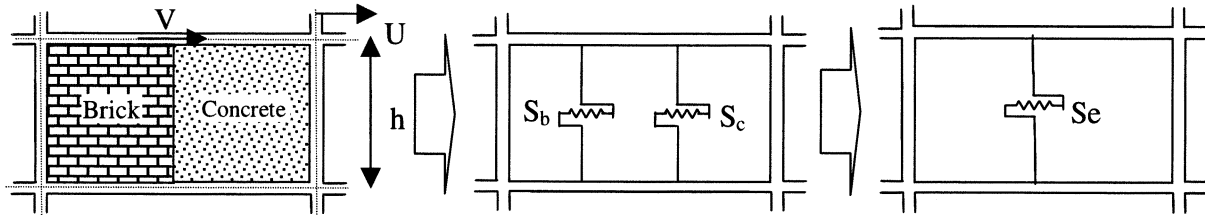


Fig. 13-g. Infill vertically multipart masonry walls Type H.

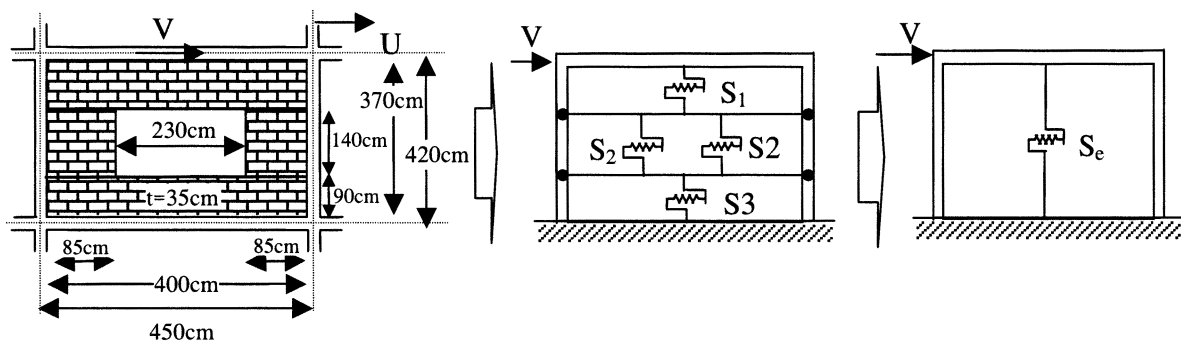


Fig. 14. An infilled frame with window opening and its equivalent with a single-spring.

in Fig. 10, for the 3D analysis of the whole building.

An example of the multi-spring infilled frame is illustrated in Fig. 14. That is type B in Fig. 13-a, which is similar to the infill masonry wall with a window opening located on the ground floor, D axis of the selected building. To obtain the force-displacement parameters of the envelope curve for each spring in the figure, first, shear strength is calculated for the infill wall without an opening as $q_m = V_m/t_l$, where, t =masonry infill masonry wall thickness, and l_m =length of infill panel. The shear stress obtained can be multiplied by t and l_m of each assumed sub-panel to obtain the shear strength for the corresponding spring. In other words, the infill wall is divided into, for this example, 3 rectangular sub-walls and then the shear strength for each sub-wall is determined individually as $V_{mi} = q_m t_i l_{mi}$, where, t_i and

l_{mi} are the thickness and the length of the sub-walls. The other parameters of sub-walls envelope curves are determined individually by equations 13 to 18. For springs S_1 , S_2 , and S_3 in Fig. 14, the maximum lateral strengths V_{mi} are calculated as: $V_{m1}=58.4$ tonf, $V_{m2}=12.4$ tonf, and $V_{m3}=58.4$ tonf, with $\alpha=0.20$. To observe the response of an infilled frame for a state in which the capacity of the infill panel has decreased to zero, it is assumed for this example that $V_{pi}=0$, $U_{pi}=2.2$ cm for all of the horizontal spring models.

The results of the pushover analysis, for the infilled frame in Fig. 14, are illustrated in Fig. 15. The figure shows the story drifts-lateral force relationships obtained for the bare frame, the infilled multi-spring frame, and the equivalent envelope single-spring. As a result, lateral strengths and correspond-

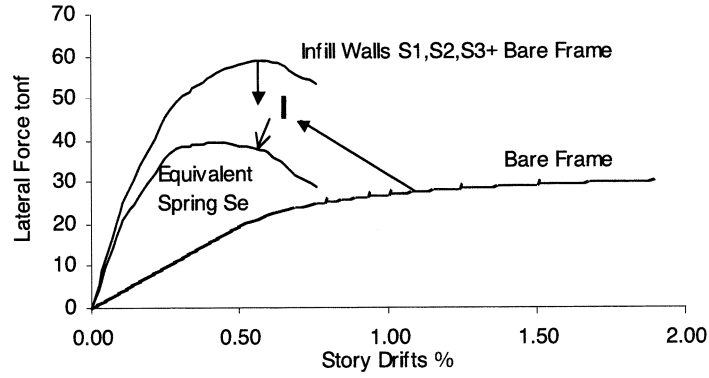


Fig. 15. Process of obtaining the envelope curve of the equivalent spring S_e by deducting the bare frame response from that of the multi-springs model.

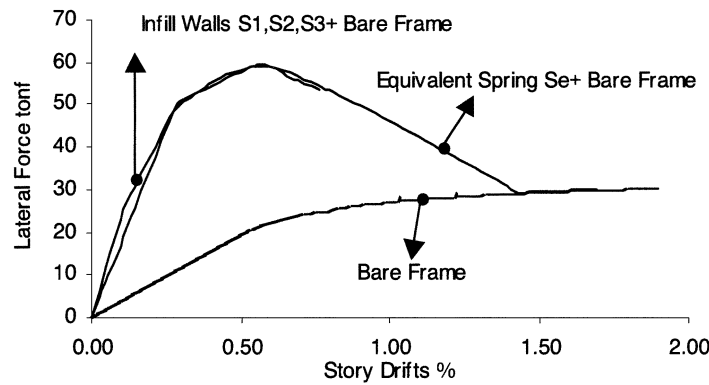


Fig. 16. Correlation of multi-spring model and equivalent single-spring model responses.

ing displacements for spring S_e are determined as : $V_y=40.3$ tonf, $U_y=1.1$ cm, $V_m=40.3$ tonf, $U_m=2.80$ cm, $U_p=5.9$ cm, and $V_{pi}=0.0$, derived from the curve obtained from the pushover analyses. To compare the results of the equivalent model to those of the multi-spring model, another pushover analysis was carried out, considering only the equivalent spring, and the results are illustrated in Fig. 16. As the results show, the multi-spring model and the single equivalent model responses are almost the same.

Pushover analyses were carried out for all of the infilled frames with openings and multi-material RC-Masonry infill walls of the selected building to obtain the equivalent single-spring models.

11. Nonlinear time-history analysis and the observed responses

The computational model of the building is developed using the modeling capabilities of the software framework of OpenSees (Mazzoni S. *et al.* 2004). The building was modeled with a 3-dimensional ide-

alization. The linear shear force-deformation relationship is chosen for columns, relying on the fact that flexural failure occurs prior to shear failure. All columns are modeled with a fiber element discrimination, with 4 monitoring sections. Infill masonry walls are modeled from an equivalent horizontal zero-length element, as described in sections 9 and 10. All beams are modeled with linear elements, as described in section 6. Reinforcing bars are assumed to be fully bonded to the surrounding concrete. Nodes at the foundation level are fixed in all degrees of freedom. The damping characteristic of the building is modeled by applying mass and stiffness proportional damping with 5% of critical damping for the first 2 modes of vibration. The first 2 natural periods of the building are estimated using an eigen-value analysis, applying the initial elastic stiffness matrix. The 2 natural periods are 0.41 and 0.40 seconds for the building with infill walls, and 0.7 and 0.5 seconds for the bare frame. The East-west, EW, direction of the building is subjected to the east-west component of

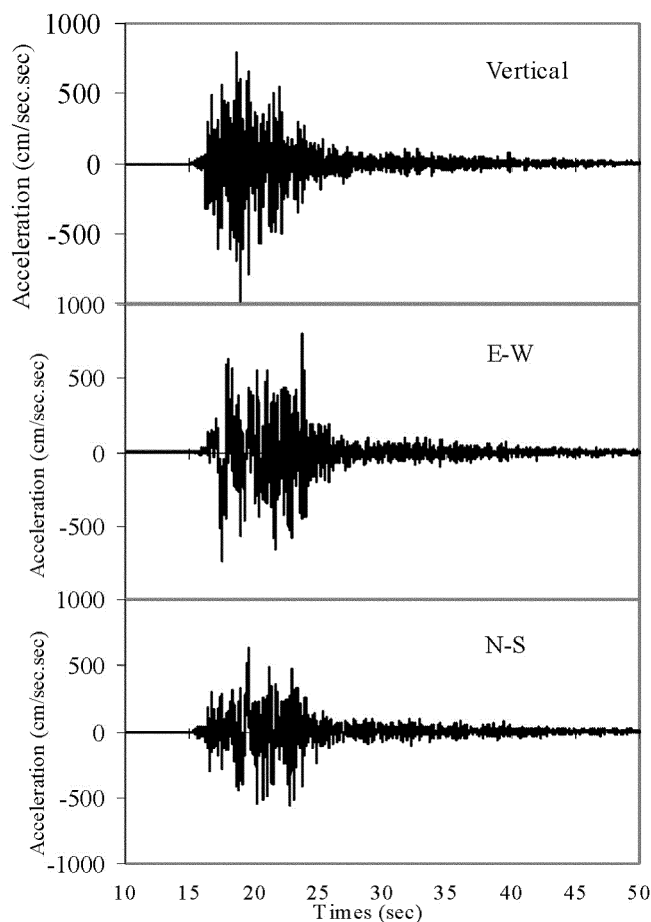


Fig. 17. Three components of strong ground motion in Bam recorded by The Building and Housing Research Center (2004).

the Bam strong motion record, E-W in Fig. 17, and north-south, NS, direction of the building is subjected to the north-south component of the record, N-S in Fig. 17. Once the vertical component of the strong motion, in addition to the other 2 components, was applied in the analysis, however no significant difference was observed, except for axis E, comparing the case with vertical component neglected. Hence, in the later analyses, the vertical component was ignored. As for axis E, which is next to a bay with a 13.2m span length, a 2D nonlinear analysis was carried out for the frame on axis 3 shown in Fig. 5-d, considering the nonlinearity of the beams, and subjected to vertical and south-north components of the earthquake. The maximum torsion about axis E due to the 2 components of the earthquake obtained was equal to 0.004 radian. Considering the height of the beam, equal to 150 cm, with parapet, the façade wall may not sustain such a perpendicular rotational angle. This might be the reason, in addition to the

lateral story drift in East-West directions, for the façade wall crashing on axis E on the top story, as shown in Figs. 1 and 26.

3 master points are introduced at the mass centers of the assumed rigid diaphragms at the 3 floor levels of the building. Displacement, velocity, and acceleration time-history responses are recorded for the all degrees of freedom. Based on the results, the maximum responses are evaluated for the east-west direction of the building. Displacements, velocity, and acceleration at the roof level in EW and NS directions for category BF, Bare Frame, category FIM, Frame and Infill Masonry, and category FIL, Frame and Infill Light panel, described in section 2, are illustrated in Figs. 18, 19, and 20. The responses, in Figs. 18 and 19, are plotted from the time step 15 seconds up to the time step 30 seconds of the strong motion records in Fig. 17 and in Figs. 20, 21, 22, and 23, from the time step 17 second to 25, to have discernible curves.

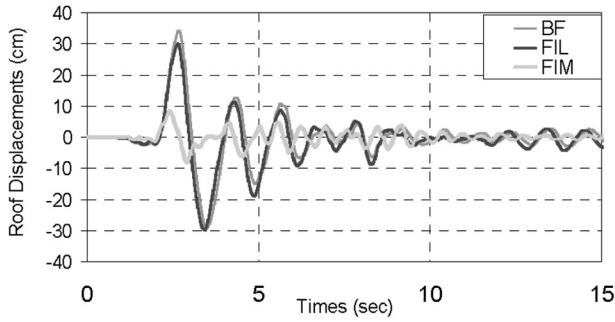


Fig. 18-a. East-west roof displacement responses.

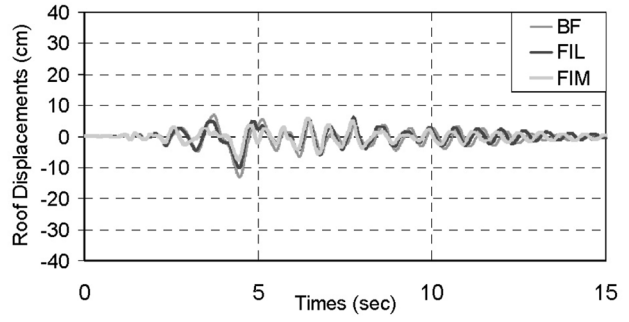


Fig. 18-b. North-South roof displacement responses.

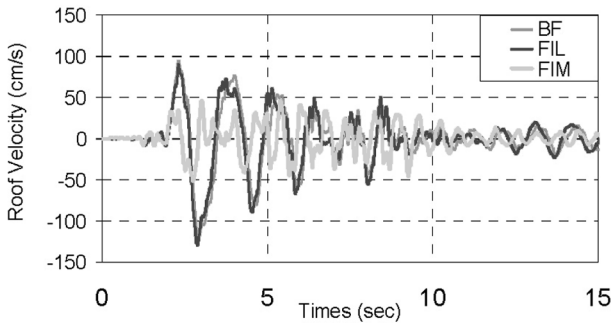


Fig. 19-a. East-west roof velocity responses.

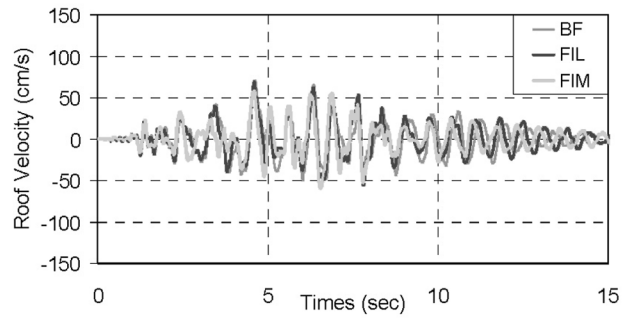


Fig. 19-b. North-South roof velocity responses.

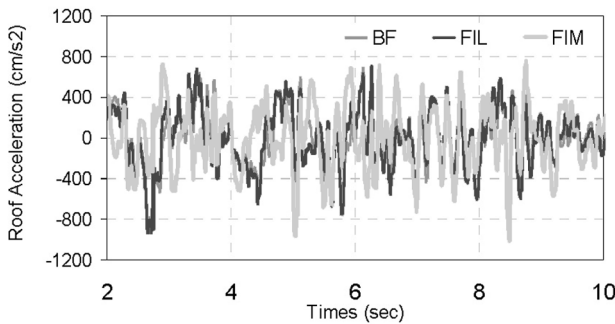


Fig. 20-a. East-west roof acceleration responses.

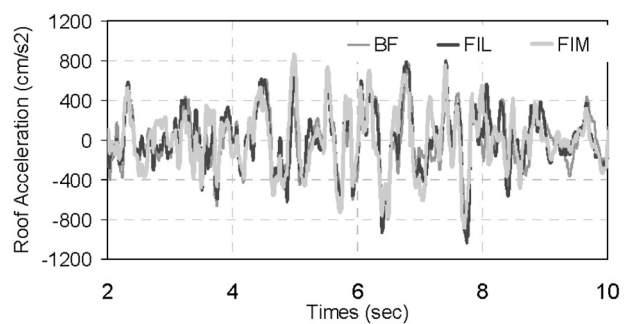


Fig. 20-b. North-South roof acceleration responses.

From the estimated responses in Figs. 18, 19, and 20, it might be considered that the building with light partitions, type FIL, has almost the same responses as those of the building with out-of-frame masonry partitions, type BF. In some of the time steps, even higher displacement responses are observed for the case of a lighter frame, type FIL, due to different frequency contents of the 2 types. However, the main differences can be observed between the infilled frame building, type FIM, and the other 2 building types, BF and FIL, as depicted in Fig. 18-a. Based on the results, maximum displacement responses in EW direction for the types BF, FIL, and FIM are

estimated as 34 cm, 30 cm and 7 cm respectively.

The ratio of maximum displacement responses of type BF to that of FIM is more than 4 times. This may imply a significant effect of the infill walls on the structural performance of the Bam Telephone Center building. In other words, large nonlinear deformations or damage could be expected in the building due to the earthquake if all the infill masonry walls were out of frame bays, or if light partitioning panels were erected in the building instead of masonry walls. Because the beams are considered to be elastic elements in the analysis, even larger nonlinear displacements compared to the responses ob-

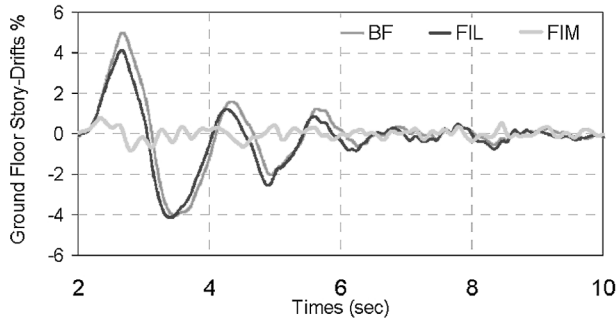


Fig. 21-a. East-west ground floor story drift ratios.

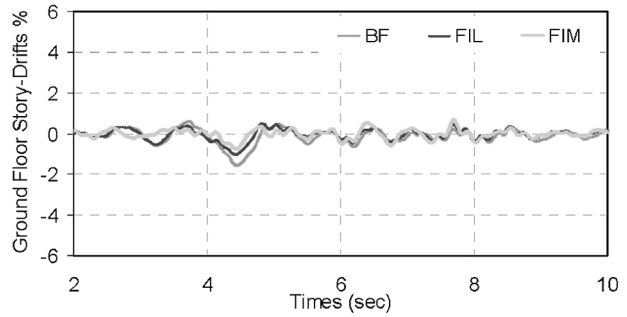


Fig. 21-b. North-South ground floor story drift ratios.

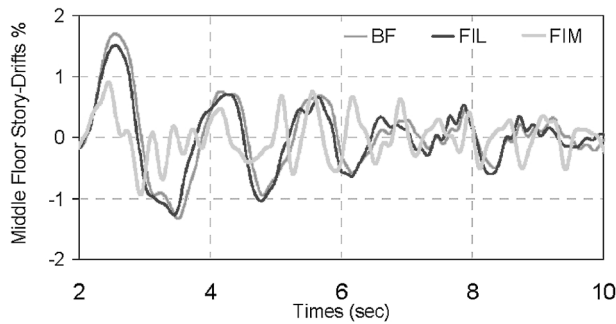


Fig. 22-a. East-west middle floor story drift ratios.

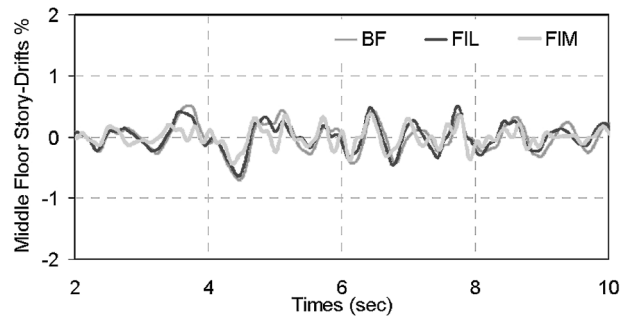


Fig. 22-b. North-South middle floor story drift ratios.

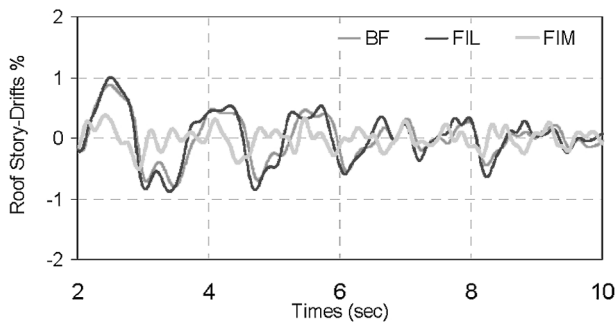


Fig. 23-a. East-west roof story drift ratios.

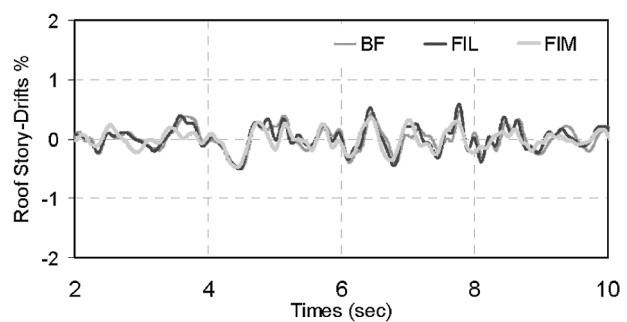


Fig. 23-b. North-South roof story drift ratios.

tained are expected for the BF type, considering the nonlinearity of the beams.

For the structural elements of the selected building, it is assumed that drift ratios less than 1% are considered as about linear states. The maximum roof displacement response of 7 cm, for FIM type, corresponds to a 0.5% drift for the total height of the building, which can be assumed as the linear state for the building. However, lateral story drifts should be checked for each floor and column to have this conclusion fulfilled. Figs. 21, 22, and 23 show time-history story drifts for the 3 categories, BF, FIL, and FIM, at the 3 floor levels.

According to the results obtained, story drifts for the 2 categories of BF and FIL are in nonlinear states in the east-west direction. However, the FIM type, which is expected to be the actual type of building, performs at all levels and directions linearly with a maximum story drift ratio of 0.8%. When comparing all of the columns story drifts for the FIM type, the maximum story drift occurred at the middle floor level of the column on A axis, in Fig. 4-b, with the value of 0.95%. These drift ratios may be considered to be linear drift ratios. Therefore, it may be concluded that the responses obtained are linear like those of the observation. It is also implied that



Fig. 24. Failure of the infill wall along the A axis in Fig. 4-b, between axis 6 and 7 in the ground floor, with corresponding maximum drift ratio of 0.9% from the analysis.



Fig. 25. The infill wall along the A axis in Fig. 4-c, between axis 6 and 7 in the top story, with corresponding maximum drift ratio of 0.1% from the analysis.

the effects of infill masonry walls would be the main factor of the linear performance of the building during the earthquake.

The infill walls damage observed is compared to those obtained by the nonlinear analysis. For solid brick masonry infill walls, a range of drift ratios of 0.15% to 0.2% for crack drift ratios, a range of 0.6% to 0.7% for drift ratios at maximum loads, and a range of 0.8% to 1% for drift ratios at 80% post-peak load level, are assumed for the comparisons, as implied from the experimental results of Mehrabi *et al.* (1996) and Chen Y.H. (2003). The story-drift ratios for different axes of the building are derived from the analysis results, and compared to the observation damages in Figs. 24 to 29. Almost in all cases the story-drift ratios are estimated to be close to the corresponding observed equivalent damage ratios.

Fig. 29 shows the façade wall of the building on axis 8 at the top story, which collapsed, probably due to the panel torsion between axes A and C. Based on the analysis, 0.1% and 0.3% drift ratios are obtained for the columns of axis A and axis C on the top story, respectively, in the east-west direction, which is the perpendicular direction of the panel. Considering the height of 200 cm for the beam and the parapet, axis 8, which can be assumed to be a rigid panel compared to that of the masonry panel, a small bending moment might be needed for crashing the façade masonry along the line of the observed collapse. The

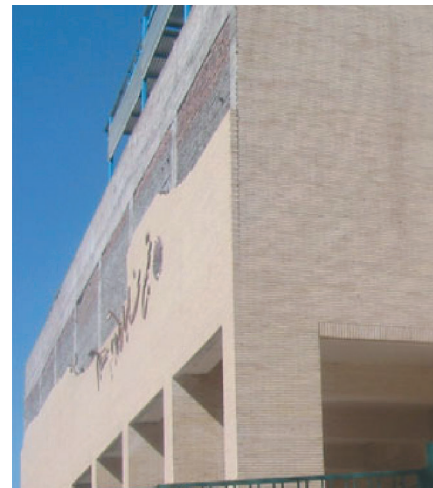


Fig. 26. Failure of the infill wall along the E axis in Fig. 4-c, top story, with corresponding maximum drift ratio of 0.15%, however, the collapse is due to torsion of the top beam, axis E next to a bay with 13.2m span length, caused by the vertical component of the earthquake, with a rotational angle of 0.4%.

same phenomenon was observed for the façade wall at axis E, as shown in Fig. 26, which is next to a bay with a 13.2 span length. However, the collapse of façade wall on axis E could be due mainly to the beam torsion caused by the vertical component of the earthquake, as explained earlier.

As can be implied from the ground floor infill wall configuration, in Fig. 3, large story drifts and

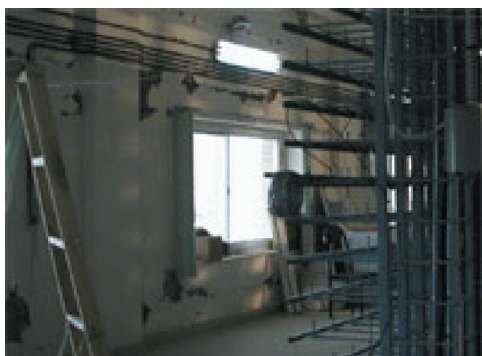
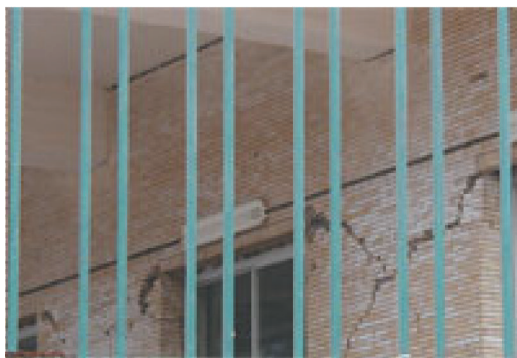


Fig. 27. Failure of the infill wall along the D axis in Fig. 4-b, Ground floor, with corresponding maximum drift ratio of 0.8%.



Fig. 28. Out of frame walls parallel to axis 1 between axis C and D, ground floor, with the maximum drift ratio of 0.9%.

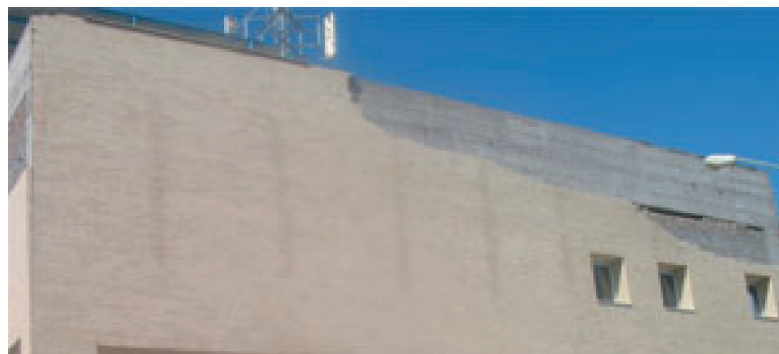


Fig. 29. Infill walls of the frames along axis 8 between axis A and E, with the maximum drift ratio of 0.25% : the collapse may be due to the panel torsion between axis A and axis C, caused by relative displacements in the perpendicular direction of the panel.

displacements are expected at this story due to the low ratio of the masonry infill wall compared to the other stories. This could be the reason why maximum story drift ratios are obtained for the ground story columns. More reductions on building displacement responses are expected if intrinsic material strengths and stiffness show higher values than those of the nominal ones.

Conclusions

A 3-dimension nonlinear analysis of the Bam telephone center-reinforced concrete building, subjected to the horizontal components of the recorded strong motion, was carried out to obtain an analytical explanation of the almost linear performance of the building during the earthquake. An approach was developed to employ analytical models for masonry infill walls with and without openings and

applied in the analysis. A significant effect of infill walls was observed on the structural response of the building. It could be concluded that the Bam telephone center building without masonry infill walls would suffer large nonlinear deformations and damage during the earthquake. The maximum overall story drift ratio of 0.8% was obtained for the ground floor of the building, which is less than a limit yielding drift ratio of 1%. Therefore, it may be concluded that the linear responses observed correlate well with the analytical results. Drift ratios for different damaged infill walls were obtained and compared to the observed responses. In most cases the comparisons lead to a fairly acceptable agreement. Further studies might be recommended for the analytical modeling of the infill walls with openings to obtain a simplified equivalent approach.

Acknowledgments

MEXT, Ministry of Education, Culture, Sport, Science and Technology of Japan sponsored the post-earthquake inspection. Architectural and structural plans and details of the building were provided by the central communication office of Kerman province in Kerman city. Technical support was provided by Iranian organizations such as Building and Housing Research Center (BHRC), National Disaster Research Institute of Iran (NDRII), and International Institute of Earthquake Engineering and Seismology (IIEES). Our thanks are extended to all those who supported completion of this study.

References

AIJ, 1994, AIJ Structural Design Guidelines for Reinforced Concrete Buildings, Architectural Institute of Japan, BHRC, 1999-a, Building and Housing Research Center,

- Minimum design load for ordinary buildings and structures, Standard 519, 2nd Edition.
 BHRC, 1999-b, Building and Housing Research Center, Iranian Code of Practice for Seismic Response Design of Buildings, Standard 2800, 2nd Edition.
 BHRC, 2004, Building and Housing Research Center, [http : //www.bhrc.gov.ir/](http://www.bhrc.gov.ir/)
 Chen, Yi-Hsin, 2003, "Seismic Evaluation of RC Buildings Infilled with Brick Walls", PhD thesis, National Cheng-Kung Univ., Tainan, Taiwan, in Chinese.
 FEMA 306, 1998, Applied Technology Council (ATC-43 Project), Evaluation of Earthquake Damaged Concrete and Masonry Wall Buildings.
 Madan A, Reinhorn AM, Mandar JB, Valles RE, 1997, Modeling of Masonry Infill Panels for Structural Analysis, *Journal of Structural Engineering ASCE* ; 123 (10) : 1295-1302.
 Mander, J. B., Priestly, M. J. N., and Park, R., 1988, Observed stress-strain behavior of confined concrete, *Journal of Structural Division, ASCE*, Vol. 114, No. 8, pp. 1827-1849
 Mazzoni S., McKenna F., Scott M. H., Fenves, G.L., Jeremic B., 2004, OpenSees Command Language Manual. PEER Center, [http : //opensees.berkeley.edu/](http://opensees.berkeley.edu/)
 Mehrabi AB, Shing PB, Shuller MP, Noland JL, 1996, Experimental Evaluation of Masonry-Infilled RC Frames, *Journal of Structural Engineering ASCE* ; 122 (3) : 228-237.
 Moghaddam, H. A., and Dowling, P.J., 1987, The state of the art in infilled frames, ESEE Research Rep. No 87-2, Civil Eng. Dept., Imperial College, London.
 Moghaddam H. A, 2004, Lateral Load Behavior of Masonry Infilled Steel Frames with Repair and Retrofit, *Journal of Structural Engineering, ASCE*, Vol. 130, No 1, 56-63
 Paulay, T., Priestley M.J.N., 1992, *Seismic Design of Reinforced Concrete and Masonry Buildings*, JOHN WILEY & SONS, INC.
 Saneinejad, A., and Hobbs, B., 1995, Inelastic Design of Infilled Frames, *Journal of Structural Engineering ASCE* ; 121 (4) : 634-650.
 Stafford-Smith and Carter, 1969, A method of analysis for infilled frames, *Proceedings of the Institute of Civil Engineers*, 44, 31-48

(Received February 17, 2005)

(Accepted February 21, 2005)